PARAMETER OPTIMISATION OF A VIRTUAL SYNCHRONOUS MACHINE IN A MICROGRID

Timo Dewenter,[1] Wiebke Heins,[2,3] Benjamin Werther,[4] Alexander K. Hartmann,[1] Christian Bohn,[2] and Hans-Peter Beck[4]

[1] *Institut für Physik, Carl von Ossietzky Universität Oldenburg, D-26111 Oldenburg, Germany*
[2] *Institut für Elektrische Informationstechnik, TU Clausthal, D-38678 Clausthal-Zellerfeld, Germany*
[3] *Zentrum für Technomathematik, Universität Bremen, D-28359 Bremen, Germany*
[4] *Institut für Elektrische Energietechnik und Energiesysteme, TU Clausthal, D-38678 Clausthal-Zellerfeld, Germany*

arXiv:1606.07357v1 [math.OC] 23 Jun 2016

Abstract

Parameters of a virtual synchronous machine in a small microgrid are optimised. The dynamical behaviour of the system is simulated after a perturbation, where the system needs to return to its steady state. The cost functional evaluates the system behaviour for different parameters. This functional is minimised by Parallel Tempering. Two perturbation scenarios are investigated and the resulting optimal parameters agree with analytical predictions. Dependent on the focus of the optimisation different optima are obtained for each perturbation scenario. During the transient the system leaves the allowed voltage and frequency bands only for a short time if the perturbation is within a certain range.

Key Words

Inverter-Based Microgrid, Virtual Synchronous Machine, Stochastic Optimisation, Parallel Tempering

1. Introduction

The number of renewable distributed energy sources (DER) has increased in the last decades forced by political, ecological, and economical aspects. Many DER are attached to the low-voltage grid by inverters, whose increased usage is accompanied by the need to find suitable control strategies and parameters for, e.g., frequency-power droop control in autonomous microgrids. Simulation methods, models and stability conditions for microgrids based on droop-controlled inverters are investigated in [1–7]. A rigorous stability

Manuscript received 23 June 2016

analysis is done in [8], in which conditions on the droop gains are derived. Simulations [9–12] have been used to obtain optimal control parameters of inverters or distributed generators in microgrids. *Particle swarm optimisation* in which a "swarm" of solutions moves in the search-space is used in [13–19].

To enhance stability in microgrids, one can use programmable inverters with storage, as e.g., the virtual synchronous machine (VISMA) [20]. It is a hysteresis controlled three-phase inverter, whose setpoints are determined by a synchronous machine model implemented on a control computer. Inertia to improve transient stability of the grid, is provided by a storage device. The VISMA is able to control (re-)active power bidirectionally and can be adjusted to meet specific power system requirements.

Here, the VISMA as grid-building element in a low-voltage islanded microgrid with voltage source inverters is investigated. The basic control strategy is droop control [6, 8] for both voltage and frequency. We use the parallel tempering method [21, 22] for optimisation of the VISMA parameters under varying transient loads (see e.g. [23]). Parallel Tempering allows to find (near-) optimal solutions for complex optimisation problems [24, 25] efficiently. The objective of our analysis is to show that the optimisation method is generally applicable to determine optimal control parameters in microgrids. Furthermore, different types of optima allow insights in the effects of the VISMA in combination with regular droop controlled inverters in microgrids for the first time.

In Sec. 2, the simulation model is described. The optimisation problem is stated in Sec. 3 and Sec. 4 explains the implementation. Results are presented in Sec. 5, a conclusion is given in Sec. 6.

2. Model of an Inverter-Based Microgrid with VISMA

2.1 Lines and Loads

Lines are modelled as algebraic equations describing the relation between voltage angles $\theta_i(t)$ and voltage magnitudes $V_i(t)$ at grid node $i \in [1,n]$ and (re-)active power flows [26]. Magnitudes and angles for all grid nodes are gathered in $V(t) = [V_1(t),\, V_2(t),\, \ldots,\, V_n(t)]^{\mathrm{T}}$ and $\theta(t) = [\theta_1(t),\, \theta_2(t),\, \ldots,\, \theta_n(t)]^{\mathrm{T}}$. The

(re-)active power injected at node i is then described by the power balance equations:

$$P_i(V(t),\theta(t)) = \quad 3\left(G_{ii}V_i^2(t) - \sum_{k\in N(i)} V_i(t)V_k(t)\left(G_{ik}\cos(\theta_i(t)-\theta_k(t)) + B_{ik}\sin(\theta_i(t)-\theta_k(t))\right)\right) \quad (1)$$

$$Q_i(V(t),\theta(t)) = \quad 3\left(-B_{ii}V_i^2(t) - \sum_{k\in N(i)} V_i(t)V_k(t)\left(G_{ik}\sin(\theta_i(t)-\theta_k(t)) - B_{ik}\cos(\theta_i(t)-\theta_k(t))\right)\right) \quad (2)$$

Here, $G_{ii} = \hat{G}_{ii} + \sum_{k\in N(i)} G_{ik}$ and $B_{ii} = \hat{B}_{ii} + \sum_{k\in N(i)} B_{ik}$, and $k \in N(i)$ denotes summation over neighbours k of node i, $\underline{\hat{Y}}_{ii} = \hat{G}_{ii} + \mathrm{j}\hat{B}_{ii}$ its shunt admittance, and $\underline{Y}_{ik} = G_{ik} + \mathrm{j}B_{ik}$ the admittance of line ik.

The load is modelled as an external disturbance $S_{\mathrm{load}}(t) = P_{\mathrm{load}}(t) + \mathrm{j}Q_{\mathrm{load}}(t)$. An algebraic constraint is introduced for the node k to which the load is connected, so $P_{\mathrm{load}}(t) = P_k(V,\theta)$, $Q_{\mathrm{load}}(t) = Q_k(V,\theta)$.

2.2 Droop-Controlled Inverters

Following [8], inverters are modelled as controllable AC voltage sources described by differential equations. Each inverter is connected to the grid via an LCL-filter with inductance L_{inv} on the inverter side, filter capacitance C_{f} and coupling inductance L_{C}. Here, $V_i(t)$ and $\theta_i(t)$ denote time-varying voltage magnitudes and angles over filter capacitances C_{f}, assuming that these are the voltages controlled by the inverter.

Droop frequency and voltage control is based on decentralized proportional controllers. Its adaption to inverter-based microgrids has been investigated [2, 4–6, 27] extensively. Because droop control is purely proportional, an offset error occurs as soon as the system is permanently disturbed. The objective of the control strategy is that in steady state (denoted by $*$) of the closed loop system devices participating in droop control share the additional (re-)active power caused by the disturbance according to the equations:

$$k_{\mathrm{P},i}\left(P_{\mathrm{nom},i} - P_i^*(V^*,\theta^*)\right) = \omega_i^* - \omega_{\mathrm{nom}}, \quad k_{\mathrm{Q},i}\left(Q_{\mathrm{nom},i} - Q_i^*(V^*,\theta^*)\right) = V_i^* - V_{\mathrm{nom}} \quad (3)$$

Here, $P_{\mathrm{nom},i}$ and $Q_{\mathrm{nom},i}$ denote the nominal active and reactive power injections of each device. V_{nom} and ω_{nom} denote the nominal voltage magnitude and frequency, respectively. The coefficients $k_{\mathrm{P},i}$ and $k_{\mathrm{Q},i}$ are parameters which determine the desired power sharing among devices. A common approach for the choice of droop coefficients $k_{\mathrm{P},i}$ and $k_{\mathrm{Q},i}$ is proportional load sharing (see [8] for analysis). Based on

the power rating S_i of each device and taking into account the legal limits for grid frequency and voltage magnitudes (49.8 Hz to 50.2 Hz, and 207 V to 253 V, respectively), we obtain:

$$k_{\mathrm{P},i} = \frac{0.4 \cdot 2\pi}{2S_i} \frac{\mathrm{rad}}{\mathrm{s}} = \frac{0.4\pi}{S_i} \frac{\mathrm{rad}}{\mathrm{s}}, \qquad k_{\mathrm{Q},i} = \frac{46\mathrm{V}}{2S_i} = \frac{23\mathrm{V}}{S_i} \quad \forall\, i \tag{4}$$

In [8], voltage source inverters are modelled with instantaneous frequency $\dot{\theta}_i(t) = \omega_{\mathrm{sp},i}(t)$, and first-order-delay voltage control $T_{\mathrm{inv}}\dot{V}_i(t) = -V_i(t) + V_{\mathrm{sp},i}(t)$, where $\omega_{\mathrm{sp},i}(t)$ and $V_{\mathrm{sp},i}(t)$ denote freely adjustable frequency and voltage setpoints. Furthermore, power measurements are processed by low-pass filters with time constants $T_i \gg T_{\mathrm{inv}}$. Choosing setpoints $\omega_{\mathrm{sp},i}(t)$ and $V_{\mathrm{sp},i}(t)$ according to (3) gives (see [8] for details):

$$\dot{\theta}_i(t) = \omega_i(t) \tag{5}$$

$$T_i\dot{\omega}_i(t) = -\omega_i(t) + \omega_{\mathrm{nom}} + k_{\mathrm{P},i}(P_{\mathrm{nom},i} - P_i(V(t),\theta(t))) \tag{6}$$

$$T_i\dot{V}_i(t) = -V_i(t) + V_{\mathrm{nom}} + k_{\mathrm{Q},i}(Q_{\mathrm{nom},i} - Q_i(V(t),\theta(t))) \tag{7}$$

2.3 The Virtual Synchronous Machine (VISMA) with Droop- and Secondary Frequency Control

The VISMA [20] is a programmable inverter which mimics the dynamics of a synchronous machine. It uses the three-phase grid voltages as input and the three-phase currents as output. Its machine model, which defines how the programmable inverter is supposed to act, is adapted to fit in the overall model:

$$\dot{\theta}_i(t) = \omega_i(t) \tag{8}$$

$$J\dot{\omega}_i(t) = -\frac{k_{\mathrm{d}}}{T_{\mathrm{d}}}\omega_i(t) - \frac{k_{\mathrm{d}}}{T_{\mathrm{d}}}d(t) + \frac{1}{\omega_i(t)}\left(P_{\mathrm{inject}}(t) - P_i(V(t),\theta(t))\right) \tag{9}$$

$$\dot{d}(t) = -\frac{1}{T_{\mathrm{d}}}\omega_i(t) - \frac{1}{T_{\mathrm{d}}}d(t) \tag{10}$$

Parameters are the virtual moment of inertia $J > 0$, the mechanical damping factor $k_{\mathrm{d}} > 0$, the damping time constant $T_{\mathrm{d}} > 0$. Compared to the VISMA model as stated in [28], this model was obtained by defining a "damping state" $d(t) = \frac{T_{\mathrm{d}}}{k_{\mathrm{d}}}M_{\mathrm{d}}(t) - \omega_i(t)$ and replacement of the momentum $M_{\mathrm{mech}}(t)$ by $M_{\mathrm{mech}}(t) = \frac{1}{\omega_i(t)}P_{\mathrm{inject}}(t)$, with $P_{\mathrm{inject}}(t)$ denoting the active power injected into the grid by the VISMA. In this setup, it is used for the purpose of droop and secondary frequency control, i.e. $P_{\mathrm{inject}}(t) = P_{\mathrm{droop}}(t) + P_{\mathrm{secondary}}(t)$.

According to (3) it is $P_{\text{droop}}(t) = P_{\text{nom},i} + \frac{1}{k_{\text{P},i}}(\omega_{\text{nom}} - \omega_i(t))$. Secondary frequency control is only performed by the VISMA and realized via an integral controller:

$$\dot{x}(t) = K_{\text{I}}(\omega_{\text{nom}} - \omega_i(t)), \quad P_{\text{secondary}}(t) = x(t) \tag{11}$$

The voltage E_{P} [28] is represented here by the voltage magnitude $V_i(t) > 0$ of the VISMA. Voltage dynamics of the VISMA are assumed as a first-order delay with a fast time constant $T_{\text{inv},i}$. A specific voltage control strategy for the VISMA [29] is implemented using the root mean square value $V_{\text{grid},i}(t)$ obtained from the grid voltage measurement between stator and grid (cf., Fig. 1) as:

$$T_{\text{inv},i}\dot{V}_i(t) = -V_i(t) + V_{\text{nom}} + k_{\text{V}}\left(V_{\text{nom}} - V_{\text{grid},i}(t)\right) \tag{12}$$

Furthermore, VISMA stator equations [28] are simplified as quasi-static and represented via an algebraic equation $\underline{Y}_{\text{VISMA}} = \frac{1}{R_{\text{S}} + \text{j}\omega L_{\text{S}}}$ with stator resistance $R_{\text{S}} > 0$ and stator inductance $L_{\text{S}} > 0$.

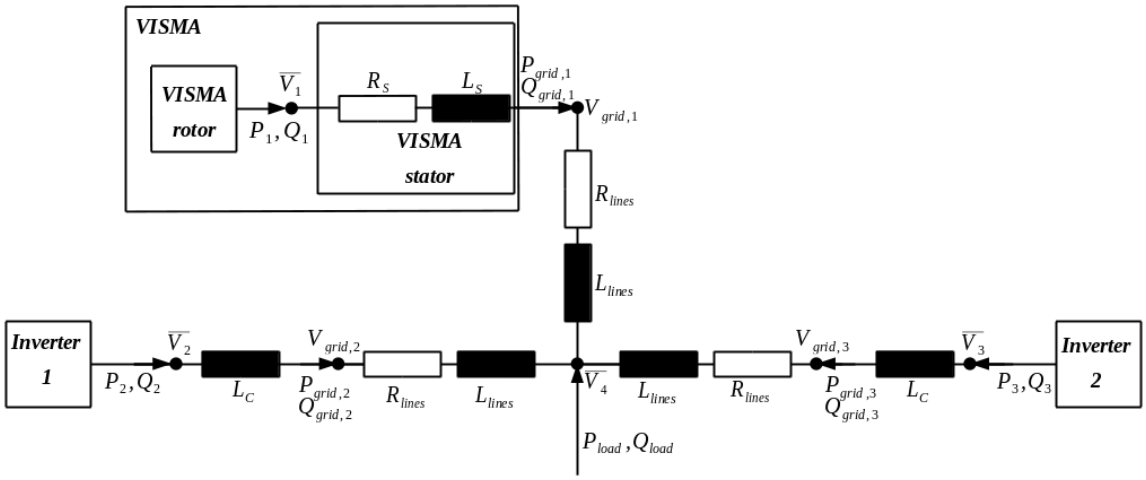

Figure 1. Scheme of the microgrid setup for simulation in perturbation scenarios.

2.4 Overall Simulation Model with Respect to a Reference Node

We choose the VISMA node (node 1) as reference node. All voltage angles are replaced by their difference to the reference node's voltage angle via $\Delta\theta_i(t) := \theta_i(t) - \theta_1(t) \,\forall\, i$. Naturally, we have $\Delta\theta_1(t) \equiv 0$ and therefore the state $\Delta\theta_1(t)$ and (8) are not needed to describe the full system. A new vector is defined for

angle states as $\Delta\theta(t) = [\Delta\theta_2(t),\ \dots,\ \Delta\theta_n(t)]^{\mathrm{T}} \in \mathbb{R}^{n-1}$. For lines and loads, $\theta_i(t)$ can be directly replaced by $\Delta\theta_i(t)\ \forall i$. For the inverters, assuming that none of them is connected to node 1, (5) is replaced by $\Delta\dot{\theta}_i(t) = \omega_i(t) - \omega_1(t)$. Given the complex power $\underline{S}_i = P_i + \mathrm{j}Q_i$, complex coupling admittance $\underline{Y}_{\mathrm{coupl}} = \frac{1}{R_{\mathrm{S}}+\mathrm{j}\omega L_{\mathrm{S}}}$ (or, for the inverters $\underline{Y}_{\mathrm{coupl}} = \frac{1}{\mathrm{j}\omega L_{\mathrm{C}}}$) and complex voltage $\underline{V_i} = V_i \mathrm{e}^{\mathrm{j}\Delta\theta_i}$, we obtain the complex voltage $\underline{V}_{\mathrm{grid},i} = V_{\mathrm{grid},i}\mathrm{e}^{\mathrm{j}\Delta\theta_{\mathrm{grid},i}}$ between VISMA stator or inverter filters and grid as $\underline{V}_{\mathrm{grid},i}(t) = \frac{|\underline{V}_i(t)|^2}{\overline{\underline{V}}_i(t)} - \frac{\overline{\underline{S}}_i(t)}{3\overline{\underline{Y}}_{\mathrm{coupl}}\overline{\underline{V}}_i(t)}$.

3. Problem Statement

3.1 Optimisation Constraints

The objective of the optimisation is to find parameters J, k_{d}, T_{d}, and K_{I} for the VISMA which positively influence the overall system behaviour after a perturbation. In order to avoid undesired or physically impossible behaviour, the optimisation variables have to be bounded by user-defined constraints.

The first constraint assures that the VISMA does not react faster than the other inverters. Therefore, we investigate the dynamics of the VISMA (cf., (9)-(10)). For the purpose of deriving a simple model as reference for the optimisation constraints, the following simplifications are used: Only the machine model is investigated, grid and stator equations, differential equations of voltage dynamics and secondary control are not considered. Taking $P_1(V(t), \Delta\theta(t))$ as system input $u(t)$, linearising around the equilibrium point $u^* = P_{\mathrm{nom},1}$, $\omega_1^* = \omega_{\mathrm{nom}}$ and $d^* = -\omega_{\mathrm{nom}}$, and applying the Laplace transform gives the transfer function:

$$G_{\mathrm{VISMA,lin}}(s) = -\frac{k_{\mathrm{P},1}(T_{\mathrm{d}}s+1)}{\frac{1}{\Omega^2}s^2 + \frac{D}{2\Omega}s + 1}, \quad c := \frac{1}{k_{\mathrm{P},1}\omega_{\mathrm{nom}}}, \quad D := \frac{\frac{1}{c}(k_{\mathrm{d}}+J)+T_{\mathrm{d}}}{2\sqrt{\frac{1}{c}JT_{\mathrm{d}}}}, \quad \Omega := \frac{1}{\sqrt{\frac{1}{c}JT_{\mathrm{d}}}} \tag{13}$$

The poles are real because $D > 1$ for any choice of parameters (proof omitted), therefore:

$$s_{\mathrm{pole},1} = -\Omega\left(D + \sqrt{D^2-1}\right), \quad s_{\mathrm{pole},2} = -\Omega\left(D - \sqrt{D^2-1}\right) \tag{14}$$

From linear system theory it is known that $\tau_{1/2} = -\frac{1}{s_{\mathrm{pole},1/2}}$ determines the exponential decay rate. This results in the constraint $\max_i(T_i) \leq \min(\tau_1, \tau_2)$, where T_i is the time constant of the regular inverters.

Assuming stable system configurations, i.e., $s_{\text{pole},1}, s_{\text{pole},2} < 0$, we conclude that $\tau_1 < \tau_2$, and therefore:

$$\max_i (T_i) \leq \frac{1}{\Omega \left(D + \sqrt{D^2 - 1} \right)} \tag{15}$$

A second constraint defines an upper bound for the parameter K_I of the integral controller (11) based on the design preference that integral control action should occur only after the first part of the transient caused by droop control is finished. For the simplified model (13) more than 95 % of the absolute value of the step size are reached after $3\max_{i=1,2}(\tau_i)$ because of the exponential character of the linearised system's step response. The response time of the integral controller should be larger. A lower bound for the response time $\frac{1}{K_\text{I}}$ of the integral controller, by using that $x(t)$ is scaled by $\frac{1}{J\omega_\text{nom}}$ in (13), is given by:

$$K_\text{I} \leq \frac{J\omega_\text{nom}}{3\tau_2} = \frac{1}{3} J\, \omega_\text{nom}\, \Omega \left(D - \sqrt{D^2 - 1} \right) \tag{16}$$

3.2 Cost Functional

The cost functional to be optimised contains three parts with parameters $\alpha > 0$ and $\beta > 0$:

$$E[\Delta f, \Delta V, \delta_\text{f}, \delta_\text{V}, \alpha, \beta] = t_\text{final} + \alpha \cdot (k_\text{d} + J) + \underbrace{(\Delta f / \delta_\text{f} + \Delta V / \delta_\text{V})}_{=:\Sigma} / \beta \tag{17}$$

α and β allow to shift the focus of the optimisation. First, we want the transient after a perturbation to be as short as possible, i.e., $t_\text{relax} \to \min$. The time t_relax is the relaxation time of the system after a perturbation. It is defined as the largest time of the moments, when the frequencies reach 49.999 Hz again. The time interval $t_\text{final} = t_\text{relax} - t_0$ considers the moment t_0 when the jump in load occurs. Second, we consider the peak depth in the transients of frequency and voltage. We want them to be as small as possible to avoid damage on electronic devices, i.e., $\Delta f / \delta_\text{f} + \Delta V / \delta_\text{V} \to \min$, where $\Delta f = \max_{\{i \in \{1,2,3\}\},\ t > t_0\}} |f_i(t) - f_i(t_0)|$ is the maximum frequency deviation, f_i being the frequency at node i. The max. voltage deviation is $\Delta V = \max_{\{i \in \{1,2,3,4\},\ t > t_0\}} |V_{\text{grid},i}(t) - V_{\text{grid},i}(t_0)|$, with grid voltage $V_{\text{grid},i}(t)$.

Third, a trade-off must be found between the required storage capacity of the VISMA, which should be as small as possible, and the energy that is used to keep up its virtual inertia. By setting $M_\text{mech} = 0$ and

integrating (9) over time, the energy provided to or taken from the microgrid by the VISMA is:

$$E_{\mathrm{VISMA}} = -\frac{1}{2}\left(J + k_{\mathrm{d}}\right)\left(\omega^2(t_2) - \omega^2(t_1)\right) + T_{\mathrm{d}} \int_{t_1}^{t_2} \omega_i(t)\, \dot{M}_{\mathrm{d}}(t)\, \mathrm{d}t \tag{18}$$

T_{d} is responsible for scaling the energy loss due to damping and the other part of the energy is dominated by $J + k_{\mathrm{d}}$. To avoid unnecessary large storage capacities $k_{\mathrm{d}} + J$ is minimised. The constraints of the optimisation problem allow some insights into the structure of the optima in advance. Choosing a very small k_{d} and T_{d} close to $\max_{i=1,2} T_i$ gives values as close as possible to the lower bound of (15). On the one hand this indicates that an optimisation with focus on keeping the transient behaviour of the VISMA close to those of regular inverters (i.e., minimising the virtual inertia $J + k_{\mathrm{d}}$ and the transient time t_{final}) will give results close to $T_{\mathrm{d}} \approx \max_{i=1,2} T_i$, $k_{\mathrm{d}} \approx 0$ and $J \approx c \max_{i=1,2} T_i$. Minimising mainly t_{final} on the other hand leads to a large value within limits given by (16), namely $K_{\mathrm{I}} \approx \frac{1}{3k_{\mathrm{P},1}}$.

4. Implementation

The energy landscape (see Fig. 2) is rough with many local minima, in particular due to a stochastic term needed for the initial conditions when solving the differential equations, preventing the application of standard, e.g., gradient-based, methods. Instead, we use Parallel Tempering here, which also works for harder optimization problems, but is easy to implement.

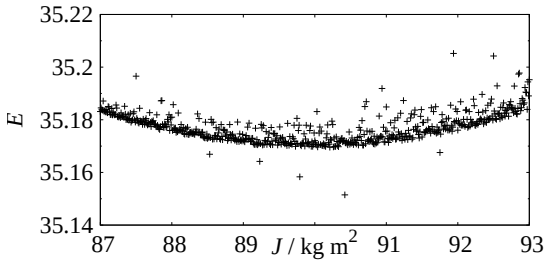

Figure 2. 2D projection of the energy landscape (value of cost functional E (17)) for scenario 1, close to Min. #2. The parameters $T_{\mathrm{d}} = 0.6$, $k_{\mathrm{d}} = 2.6 \cdot 10^{-4}$, and $K_{\mathrm{I}} = 1060$ are fixed, whereas J is varied.

4.1 Parallel Tempering

The optimisation algorithm works as follows. The configurations of the system are sampled according to the Boltzmann probability distribution $P(E_i) = 1/Z \exp(-E_i/\Theta)$, where Z is a normalization constant,

E_i is the energy of configuration i and Θ an artificial temperature. This is achieved via a special Monte Carlo (MC) sampling, the Metropolis alogrithm [30], where in each iteration, a new candidate configuration with corresponding energy E_2 is created and accepted with probability:

$$p_{\text{Metr}} = \min\left\{1, e^{-(E_2-E_1)/\Theta}\right\} \tag{19}$$

E_1 is the energy of the current state. As (19) fulfills *detailed balance*, sampling according to a Boltzmann distribution is ensured. From physics we know that for $\Theta \to 0$, the energy obtains a minimum $E \to E_{\min}$. This leads to the idea of *Simulated Annealing* [31], where the temperature of an MC simulation is gradually decreased until a minimum is found. This approach can get stuck in a local minimum. An improvement is to simulate the system at various temperatures Θ_i. This can be done by Parallel Tempering [21, 22], where a random walk in temperature space is performed. To preserve detailed balance and equilibrium for an infinite number of iterations, the Metropolis criterion [21] with energies $E(\cdot)$ is used:

$$p_{\text{Swap}} = \min\left\{1, \exp\left(\left[\frac{1}{\Theta_k} - \frac{1}{\Theta_{k+1}}\right][E(y_k) - E(y_{k+1})]\right)\right\} \tag{20}$$

Two neighbouring configurations with temperatures Θ_k, Θ_{k+1} ($k \in [1, n-1]$) can be exchanged. In each such *swap*, $k \in \{1,2,3,\ldots,n-1\}$ is chosen at random with equal probability.

4.2 Implementation of the Optimisation Algorithm

Within an optimisation procedure, one of two perturbation scenarios is considered. Both are based on a step in load. During the transient it is checked whether the usual frequency and voltage ranges are met (see (4)). If these are not fulfilled, the parameter set is rejected, i.e., $E = \infty$. Before (17) is calculated in the simulation, the constraints (15) and (16) are checked. If they are not fulfilled, the parameter set is rejected.

We use from the GSL [32]: A hybrid method (Newton and dogleg step) for solving the steady state equations, where the results are used as initial conditions for the Runge-Kutta-Fehlberg method to solve the differential equations. For parallelization we use OpenMPI [33]. The 12 temperatures used in the

simulations are $\Theta_i \in \{0.01, 0.02, 0.07, 0.2, 0.5, 1, 3, 7, 20, 50, 100, 10^9\}$, where 10^9 corresponds to the acceptance of every new state except the ones that violate (15), (16) or lead to an unstable system state. For each temperature Θ_i the MC sampling is performed in the following way:

1. Calculate value of cost functional E_1 with given parameter set $\Phi = (J, k_\mathrm{d}, T_\mathrm{d}, K_\mathrm{I})$.
2. Choose one parameter O of the four parameters from Φ with equal probability at random.
3. Calculate $O' = O \cdot m$ with $m = |1 + R_\mathrm{perc} \cdot r|$, where $r \in [-1, 1]$ is a random number.
4. Calculate new value of E_2 with modified parameter set Φ' in which O has been replaced by O'.
5. Accept the new parameter set Φ' with Metropolis probability (19).

The steps 2.-5. are repeated $N_\mathrm{params} \cdot 2 = 4 \cdot 2 = 8$ times. After two such *sweeps* are performed for each temperature, $n-1$ swap attempts are done. For each of these attempts the procedure is the following: First, choose a configuration $k \in [1, n-1]$ uniformly at random. Then, exchange the two configurations y_k and y_{k+1} with the swap probability given by (20). For each parameter set (α, β), 200 swaps are performed with $R_\mathrm{perc} = 0.8$. The minimum of E is found by taking the minimum of all temperatures Θ_i leading to Φ_min. Another simulation [34] with Φ_min as initial parameter set is started with 200 swaps and $R_\mathrm{perc} = 0.4$.

5. Results

5.1 Optimisation Results for Different Perturbation Scenarios

For the optimisation a microgrid in a radial topology and in island mode is considered, see Fig. 1. We neglect ohmic grid losses and focus on the frequency peak, i.e., $\delta_\mathrm{V} = 10^{40}$. The perturbation is a jump in active load. Table 1 shows the parameters that remain the same for all scenarios.

Table 1
Parameters Used for the Optimisation in All Scenarios. Values for $T_{2/3}$ taken from [8]

L_lines	L_S	R_lines	R_S	L_C	T_1	$T_{2/3}$	k_V	$Q_\mathrm{nom,1/2/3}$	K_awu
1.514 mH	42.0 mH	0.0 Ω	0.3 Ω	1.8 mH	0.01 s	0.5 s	10.0 $\frac{\mathrm{V}}{\mathrm{V}}$	0.0 var	1.0 $\frac{1}{\mathrm{s}}$

5.1.1. Scenario 1: Symmetric nominal power, load jump of 3 kW

In this scenario, a step decrease of the load power is done. See Table 2 for all parameters. In the last three columns of Table 3 the values of the parts of the cost functional (17) are given, which reflect on which part of the functional the optimisation has been focused. For the first minimum (#1) the three parts of (17) have the same weight, the second minimum (min.) focuses on t_{final}, the third on the value of $J + k_{\text{d}}$, and the fourth on small frequency peaks (Σ). For the second, third and forth min. the focus is reflected in the result, i.e., min. #2 has the smallest value of t_{final}, min. #3 the smallest of $J + k_{\text{d}}$. Min. #4 gives a comparably small value for Σ, but apparently only a local min. was found, since in min. #2 it is even smaller.

Table 2
Parameters Used for the Optimisation in Scenario 1

$S_{1/2/3}$	$P_{\text{nom},1/2/3}$	$k_{\text{P},1/2/3}$	$k_{\text{Q},2/3}$	P_{load} before jump	P_{load} after jump
4000.0 VA	500.0 W	$3.1416{\cdot}10^{-4}\ \frac{\text{rad}}{\text{s VA}}$	$5.75{\cdot}10^{-3}\ \frac{\text{V}}{\text{VA}}$	1500.0 W	4500.0 W

Table 3
Optimal Parameter Sets for Scenario 1 ($R_{\text{perc}} = 0.4$, Focus on Frequency Peak: $\delta_{\text{f}} = 0.05$, $\delta_{\text{V}} = 10^{40}$). Errors of E Resulting from 50 Runs with Different Initial Conditions.

#	J	$k_{\text{d}}/10^{-4}$	T_{d}	K_{I}	E	α	β	$J+k_{\text{d}}$	Σ	t_{final}	$\alpha(J+k_{\text{d}})$	Σ/β
1	5.0895	1.1857	0.5029	1054.56	108.93(6)	7	0.027	5.090	0.994	36.483	35.627	36.820
2	91.479	2.5800	0.5917	1060.97	35.12(2)	0.07	2.7	91.480	0.817	28.415	6.4036	0.3026
3	5.0692	1.0071	0.5163	975.67	3624.89(9)	700	0.027	5.069	1.000	39.379	3548.494	37.026
4	50.894	10.1498	1.2539	1053.54	3425(46)	7	$2.7 \cdot 10^{-4}$	50.895	0.820	32.913	356.265	3036.54

In Sec. 3.2 it was stated that $T_{\text{d}} \approx \max_{i=1,2} T_i = 0.5$, $k_{\text{d}} \approx 10^{-4}$ (since it is bounded by this value) and $J \approx c \max_{i=1,2} T_i \approx 10.13 \cdot 0.5 \approx 5.07$ in cases where $J + k_{\text{d}}$ and t_{final} are minimised with equal weighting, and $K_{\text{I}} \approx \frac{1}{3k_{\text{p},1}} \approx 1061.03$, if the minimisation focuses on t_{final}. These values are close to min. #1 and #3, and min. #2 for focussing on t_{final}. Weightings on other parts of the cost functional (e.g., min. #4) lead to minima which are further away from the bounds of the optimisation constraints.

The results from Table 3 are visualized (see Fig. 3) by a comparison for VISMA frequencies and voltages for all four minima. The remaining grid values are shown only for the first minimum, see Fig. 4.

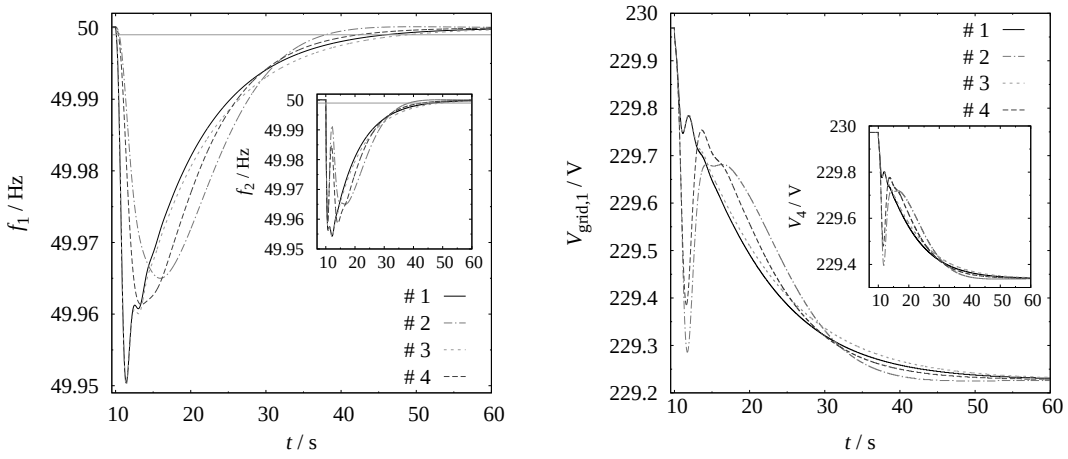

(a) Frequencies. (b) Voltages.

Figure 3. Comparison of the four minima for scenario 1 given in Table 3.

5.1.2. Scenario 2: Different nominal powers and load jump of 7 kW

In this scenario, we assume different rated and nominal active powers of the devices (see Table 4). The optimal parameter sets obtained for this setup are shown in Table 5. Fig. 5 shows the system behaviour for min. #1 of Scenario 2. Different time constants of the VISMA and the two inverters cause a different system behaviour than in Scenario 1. The VISMA's reaction is very slow due to its high virtual inertia (for min. #1, $J \approx 11.5$). Directly after the load jump the inverters have to balance the sudden power demand. This forces them to provide active power at a value (~ 8 kW) above their nominal rated power values $S_{2/3}$. Inverters for island grids allow this for a short amount of time.

Table 4
Parameters Used for the Optimisation in Scenario 2

S_1	S_2	S_3	$P_{\text{nom},1}$	$P_{\text{nom},2}$	$P_{\text{nom},3}$	$k_{\text{P},1}$	$k_{\text{P},2}$
9.0 kVA	3.0 kVA	1.0 kVA	1.0 kW	1.5 kW	0.5 kW	$1.3963{\cdot}10^{-4}$ $\frac{\text{rad}}{\text{s VA}}$	$4.1888{\cdot}10^{-4}$ $\frac{\text{rad}}{\text{s VA}}$

$k_{\text{P},3}$	$k_{\text{Q},2}$	$k_{\text{Q},3}$	P_{load} before jump	P_{load} after jump
$12.5664{\cdot}10^{-4}$ $\frac{\text{rad}}{\text{s VA}}$	$7.67{\cdot}10^{-3}$ $\frac{\text{V}}{\text{VA}}$	$23.0{\cdot}10^{-3}$ $\frac{\text{V}}{\text{VA}}$	3.0 kW	10.0 kW

Despite the different system behaviour compared to Scenario 1, the effect of the optimisation with different weights is clearly reflected in the values of the cost functional (see Table 5). The very small t_{final} for min. #2 is due to an overshoot in frequencies (figure not shown): After reaching 49.999 Hz for the first

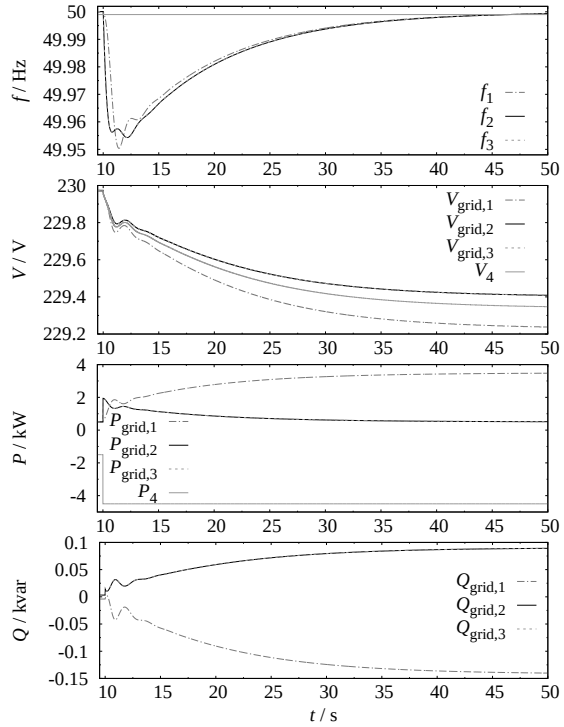

Figure 4. Minimum #1 of scenario 1.

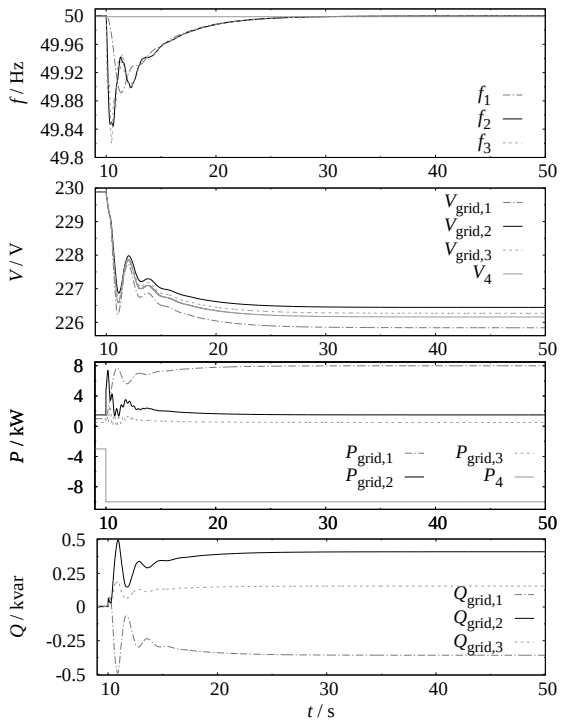

Figure 5. Minimum #1 of scenario 2.

Table 5
Optimal Parameter Sets for Scenario 2 ($R_{\mathrm{perc}} = 0.4$, Focus on Frequency Peak: $\delta_{\mathrm{f}} = 0.2$, $\delta_{\mathrm{V}} = 10^{40}$). Errors of E Resulting from 50 Runs with Different Initial Conditions.

#	J	$k_{\mathrm{d}}/10^{-4}$	T_{d}	K_{I}	E	α	β	$J+k_{\mathrm{d}}$	Σ	t_{final}	$\alpha(J+k_{\mathrm{d}})$	Σ/β
1	11.4986	1.1595	0.5035	2379.26	59.26(1)	1.7	0.045	11.499	0.902	19.671	19.548	20.046
2	59.3043	4.2760	0.9356	2387.04	14.99(1)	0.017	4.5	59.305	0.887	13.781	1.0082	0.1971
3	11.4076	1.0139	0.5064	2348.85	1979.32(1)	170	0.045	11.408	0.902	19.967	1939.309	20.040
4	16.8974	13.2759	0.6524	2382.76	2039.5(5)	1.7	$4.5 \cdot 10^{-4}$	16.899	0.896	19.076	28.728	1991.7

time, f_1 leaves the range of $[49.999, 50.001]$ again before returning to 50 Hz. Optimisations for the same scenarios with ohmic losses in lines have been performed (results not shown). Though transients show different characteristics, almost the same parameter sets are found.

6. Conclusion

Parameters of a VISMA in an islanded microgrid with radial topology containing two inverters and a load have been optimised using Parallel Tempering. By varying additional parameters in the cost functional the focus of the optimisation was shifted. For two perturbation scenarios minima of the cost functional were found which are stable solutions within the prescribed boundaries. The results show that this optimisation

procedure is in general applicable to the task of parameter optimisation in a microgrid. It is also shown that through the proper setting of the VISMA's parameters its functionality can be adapted to different participants in the grid. The values obtained by analytical investigation in 3.2 seem to offer a "rule of thumb" for a good parameter region. However, the effects of each parameter in complex situations are not obvious. For other topologies, devices or disturbances, totally different parameter sets might be needed. In order to find a good parameter set for a given microgrid setup, various disturbances should be analyzed.

In future research, other forms of the constraints for the VISMA parameters and cost functionals should be investigated. Larger microgrids with other power generating systems can be put under scrutiny. The proposed approach could be transferred to the optimisation of parameters in other control strategies. An extension would be the study of different disturbance scenarios, where one uses e.g., a series of steps in load. Finally, theoretical results should be confirmed by measurements in an appropriate laboratory.

Acknowledgment

Simulations were performed at the HERO cluster of the Carl von Ossietzky Universität Oldenburg, funded by the DFG through its Major Research Instrumentation Programme (INST 184/1081 FUGG) and the Ministry of Science and Culture of the Lower Saxony State. Financial support was obtained by the Lower Saxony research network "Smart Nord" which acknowledges the support of the Lower Saxony Ministry of Science and Culture through the "Niedersächsisches Vorab" grant programme (grant ZN2764).

References

[1] N. Pogaku, M. Prondanovic, & T. Green, Modeling, analysis, and testing of autonomous operation of an inverter-based microgrid, *IEEE Trans. Power Electron.*, *22*, 2007, 613.

[2] E. Coelho, P. Cortizo, & P. Garcia, Small signal stability for parallel connected inverters in stand-alone AC supply systems, *IEEE Trans. Ind. Appl.*, *38*, 2002, 533.

[3] M. Marwali, J. Jung, & A. Keyhani, Stability analysis of load sharing control for distributed genera-

tion systems, *IEEE Trans. Energy Convers.*, *22*, 2007, 737.

[4] E. Barklunk *et al.*, Energy management in autonomous microgrid using stability-constrained droop control of inverters, *IEEE Trans. Power Electron.*, *23*, 2008, 2346.

[5] N. L. Soultanis, S. A. Papathanasiou, & N. D. Hatziargyriou, A stability algorithm for the dyn. analysis of inv. dominated unbalanced LV MGs, *IEEE Trans. Power Syst.*, *22*(1), 2007, 294–304.

[6] A. Engler, Applicability of droops in low voltage grids, *DER Journal*, *1*, 2005, 1.

[7] J. W. Simpson-Porco, F. Dörfler, & F. Bullo, Synchronization and power sharing for droop-controlled inverters in islanded microgrids, *Automatica*, *49*(9), 2013, 2603 – 2611.

[8] J. Schiffer *et al.*, Cond. for stab. of droop-contr. inv.-based MGs, *Automatica*, *50*, 2014, 2457–2469.

[9] A. Raghami, M. T. Ameli, & M. Hamzeh, Online droop tuning of a multi-DG microgrid using cuckoo search algorithm, *Electr. Pow. Compo. Sys.*, *43*(14), 2015, 1583–1595.

[10] R. Godoy *et al.*, Different.-evolution-based optim. of the dyn. response for parallel oper. of inv. with no controller interconnection, *IEEE Trans. Ind. Electron.*, *59*, 2012, 2859.

[11] S. Mishra, G. Mallesham, & A. Jha, Design of controller and communication for frequency regulation of a smart microgrid, *IET Renewable Power Gener.*, *6*, 2011, 248.

[12] M. J. Sanjari & G. B. Gharehpetian, Game-theoretic appr. to coop. control of distrib. energy resources in islanded MG considering voltage and frequency stab., *Neural Comput. Appl.*, *25*, 2013, 343.

[13] I.-Y. Chung, W. Liu, D. A. Cartes, & S.-I. Moon, Control parameter optim. for multiple distr. generators in a MG using particle swarm optimization, *Eur. Trans. Electr. Power*, *21*, 2011, 1200.

[14] M. Hassan & M. Abdio, Optimal design of microgrids in autonomous and grid-connected modes using particle swarm optimization, *IEEE Trans. Power Electron.*, *26*, 2011, 755.

[15] W. Al-Saedi, S. Lachowicz, D. Habibi, & O. Bass, Power quality enhancement in auton. MG operation using particle swarm optimization, *Int. J. Electr. Power Energy Syst.*, *42*, 2012, 139.

[16] H. Bevrani *et al.*, Intelligent frequency control in an AC microgrid: Online PSO-based fuzzy tuning approach, *IEEE Trans. Smart Grid*, *3*, 2012, 1935.

[17] L. Yu *et al.*, A novel information exchange particle swarm optimization for MG multi-objective dynamic optimization control, *J. Renew. and Sustain. Ener.*, *6*(2), 2014, 023114.

[18] Y. Zeng & S. Yanguang, Enhanced multi-objective particle swarm opt. for opt. reactive power dispatch considering voltage stability, *Int. J. of Power and Energy Systems*, *34*, 2014, 116–24.

[19] P. Wang *et al.*, Control parameter optimization for AP1000 reactor using particle swarm optimization, *Ann. Nucl. Energy*, *87, Part 2*, 2016, 687 – 695.

[20] H.-P. Beck & R. Hesse, Virtual synchronous machine, *IEEE 9th Intern. Conf. on Electrical Power Quality and Utilisation (EPQU)*, Barcelona, Spain, 2007.

[21] K. Hukushima & K. Nemoto, Exchange monte carlo method and application to spin glass simulations, *J. Phys. Soc. Jpn.*, *65*, 1996, 1604.

[22] R. H. Swendsen & J.-S. Wang, Replica MC simul. of spin-glasses, *Phys. Rev. Lett.*, *57*, 1986, 2607.

[23] M. S. Rahman Tito, T. T. Lie, & T. Anderson, Sizing optimization of wind-photovoltaic hybrid energy sys. under transient load, *Int. J. of Power and Energy Systems*, *33*, 2013, 168–74.

[24] A. K. Hartmann & H. Rieger, *Optim. Algor. in Physics*, (Berlin: Wiley-VCH, 2001), 1st edition.

[25] A. K. Hartmann & H. Rieger (Eds.), *New Optim. Algor. in Physics*, (Weinheim: Wiley-VCH, 2004).

[26] P. Kundur, *Power System Stability and Control*, (New York: McGraw-Hill, 1994).

[27] M. Chandorkar, D. Divan, & R. Adapa, Control of parallel connected inverters in standalone AC supply systems, *IEEE Trans. Ind. Appl.*, *29*(1), 1993, 136–143.

[28] T. Dewenter, B. Werther, A. K. Hartmann, & H.-P. Beck, Optim. des dyn. Verhaltens netzstützender Anlagen am Bsp. der VISMA (Optim. of the dyn. behavior of grid-supporting devices for the example of the VISMA), *Proc. 13. Symp. Energieinnov. (EnInnov2014)*, Graz, Austria, 2014.

[29] Y. Chen, R. Hesse, D. Turschner, & H.-P. Beck, Improving the grid power quality using VISMAs, *Intern. Conf. on Power Engin., Energy and Electr. Drives (POWERENG)*, Malaga, Spain, 2011.

[30] N. Metropolis *et al.*, Eq. of state calcul. by fast comput. mach., *J. Chem. Phys.*, *21*, 1953, 1087–1092.

[31] S. Kirkpatrick, C. D. Gelatt, & M. P. Vecchi, Optimization by simulated annealing, *Science*, *220*(4598), 1983, 671–680.

[32] M. Galassi *et al.*, *GNU Scientific Library Reference Manual*, 3rd edition, 2009.

[33] E. Gabriel *et al.*, Open MPI: Goals, concept, and design of a next genereration MPI implementation, *Proc. 11th Europ. PVM/MPI Users' Group Meet.*, Budapest, Hungary, 2004.

[34] A. K. Hartmann, *Big Practical Guide to Computer Simulations*, (Singapore: World Scientific, 2015).